WILEY InterScience® DISCOVER SOMETHING GREAT

PROTEINS STRUCTURE ■ FUNCTION ■ BIOINFORMATICS

A molecular dynamics study comparing a wild-type with a multiple drug resistant HIV protease: Differences in flap and aspartate 25 cavity dimensions

Steve A. Seibold and Robert I. Cukier*

Department of Chemistry, Michigan State University, East Lansing, Michigan 48824-1322

ABSTRACT

HIV proteases can develop resistance to therapeutic drugs by mutating specific residues, but still maintain activity with their natural substrates. To gain insight into why mutations confer such resistance, long (~70 ns) Molecular Dynamics simulations in explicit solvent were performed on a multiple drug resistant (MDR) mutant (with Asn25 in the crystal structure mutated* in silico *back to the catalytically active Asp25) and a wild type (WT) protease. HIV proteases are homodimers, with characteristic flap tips whose conformations and dynamics are known to be important influences of ligand binding to the aspartates that form the catalytic center. The WT protease undergoes a transition between 25 and 35 ns that is absent in the MDR protease. The origin of this distinction is investigated using principal component analysis, and is related to differences in motion mainly in the flap region of each monomer. Trajectory analysis suggests that the WT transition arises from a concerted motion of the flap tip distances to their catalytic aspartate residues, and the distance between the two flap tips. These distances form a triangle that in the WT expands the active site from an initial (semi-open) form to an open form, in a correlated manner. In contrast, the MDR protease remains in a more closed configuration, with uncorrelated fluctuations in the distances defining the triangle. This contrasting behavior suggests that the MDR mutant achieves its resistance to drugs by making its active site less accessible to inhibitors. The migration of water to the active site aspartates is monitored. Water molecules move in and out of the active site and individual waters hydrogen bond to both aspartate carboxylate oxygens, with residence times in the ns time regime.

Proteins 2007; 69:551–565.

***Key words:** HIV protease; molecular dynamics; principal component analysis; multiple drug resistant.*

INTRODUCTION

HIV protease is an essential component in the replication of the virus that causes AIDS.[1] It activates other HIV proteins by cleaving the nascent viral polyprotein chain at specific sites to produce active proteins. Numerous crystal structures have been obtained, leading to the discovery of the active site, and the prediction that the enzyme utilizes an aspartic protease acid-base mechanism for protein cleavage.[2–8] However, the structural/conformational changes that are required for binding of substrate, its cleavage, and release of product are still obscure.

The HIV protease [Fig. 1(A)] is a 22 kDa homodimer. The scaffolding of the active site, formed by the homodimer's interface, contains two β-hairpin loops and two flexible β-hairpin structures or "flaps" that close down on the active site upon substrate binding and open up for product release. Each 99-residue monomer contributes a catalytically essential aspartic acid (Asp25) as part of the conserved Asp-Thr-Gly sequence.[9]

The variations in flap conformations observed in X-ray studies of the protease suggest that the flaps are flexible and can adopt multiple conformations.[10] NMR studies demonstrated that the flap tips (residues 46–54) are, indeed, mobile on the micro-second and sub-nanosecond time scales and move from one extreme (closed) to another (open).[11] As important as these observations are, they do not provide atomic details about the role of the atoms or residues in the flap movements, which are essential for understanding their function in substrate interaction and in drug resistance. The flap tips, containing the hydrophobic sequence GGIGG, are highly mobile, which is consistent with the presence of flexible residues such as glycine. Scott and Schiffer[12] suggest that curling of the flap tips occurs to bury hydrophobic residues and aids in substrate entry to the catalytic site. A mechanism for increasing the conformational flexibility of the glycine rich flap tips was elucidated by free energy simulations.[13] Meagher and Carlson[14] simulated HIV protease and compared the MD flap fluctuation order

*Correspondence to: Robert I. Cukier, Department of Chemistry, Michigan State University, East Lansing, MI 48824-1322.
E-mail: cukier@cem.msu.edu
Received 30 October 2006; Revised 21 February 2007; Accepted 22 March 2007
Published online 10 July 2007 in Wiley InterScience (www.interscience.wiley.com).
DOI: 10.1002/prot.21535

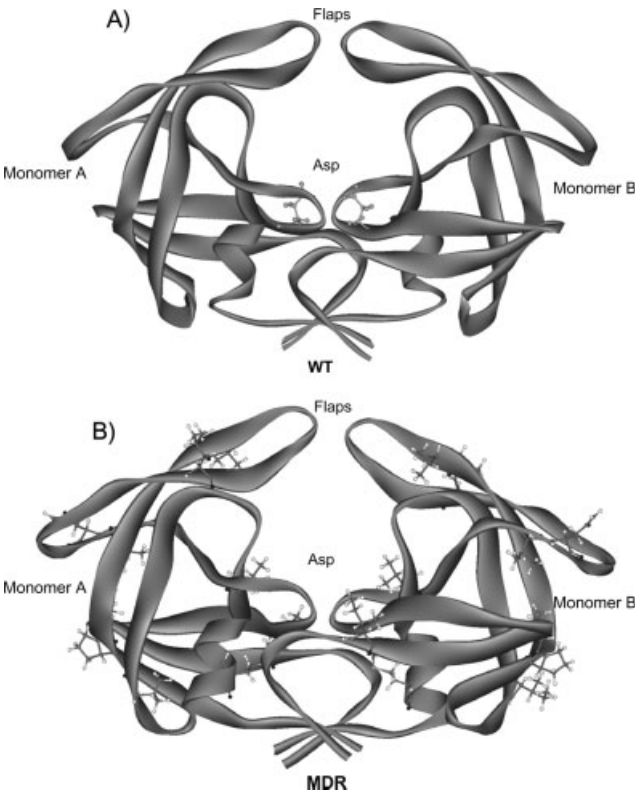

Figure 1

*Homodimer crystal structures of (**A**) WT (1hhp) and (**B**) MDR HIV Protease (1RPI). In (A), the catalytic aspartates (Asp25 and Asp124) are displayed in ball and stick,. The MDR structure also shows the mutations that lead to MDR behavior in ball and stick. Note that (see Methods) the MDR was mutated* in silico *from Asn to Asp for our simulation.*

parameters with those from NMR experiments. It is evident that the behavior and positioning of these residues will play a key role in substrate access to the enzyme[15] and, possibly, in catalysis. Mutations in this region can disrupt enzyme activity and, in addition, may impart drug resistance.[16–19]

Since the protease is such an essential part of the HIV life cycle, many drugs have been tested for their ability to interact with and inhibit it. However, the enzyme mutates at numerous sites at such a rapid rate that HIV protease becomes drug resistant in many individuals.[9,20] Such mutations can even lead to multiple drug resistant (MDR) strains.[9,10,20] Variants of HIV are able to evolve MDR inhibitor resistance by complementary strategies such as combinations of active-site and nonactive-site mutations [Fig. 1(B)]. Some combinations of these mutations reduce the affinity for both inhibitors and substrate most probably by disrupting favorable binding interactions.[21,22] Conversely, some "compensatory mutations" are able to enhance the protease activities that have been originally decreased by active-site mutations.[9,23]

The mechanism behind MDR inhibition is not well understood, but the variants do have mutations in both the active site and nonactive site regions. The inhibition can be accomplished by disturbing favorable ligand protein interactions in the binding pocket. However, accumulating evidence suggests that the flap region also plays an important role in influencing both substrate and inhibitor binding/stability.[12,24] Indeed, some "compensatory" mutations occurring in the flap region can restore activity that was disrupted by an earlier active-site mutation.[23,24] Although the flap mechanism of HIV activity and inhibition is not known, it has been postulated that the HIV protease's flaps partition between an open and closed form (closed corresponding to a ligand-bound structure) where the flaps can move as much as 15 Å.[25–27] The ability of certain mutants to alter the equilibrium between the open and closed conformations, or to favor a semi-open form (defined to correspond to the apo protease conformation), may produce the drug resistant form of the enzyme.[26,28] Another possibility for MDR is that the active site specificity itself is reduced because of a mutation(s) in the catalytic site, inducing an expansion of the active site. It has been suggested that some HIV MDR mutants have a decrease in the volume of amino acid side chains within the active-site cavity because of direct residues changes in the active site itself and/or by mutations in the flap region preventing flap closure. This expanded active site reduces the fit of inhibitors and lowers the binding affinity by decreasing van der Waals contacts and hydrogen bonding.[24,29]

In addition to the role of crystallographic waters found in HIV-protease in the presence of inhibitors, simulations have also been carried out with added waters to investigate their mechanistic role.[30–33] It has been demonstrated that water is involved by mediating inhibitor binding, and in linking the flap regions together with and without inhibitors.[32,34] Certain inhibitors may impede activity by filling the catalytic site with an inhibitor hydroxyl group.[10,30,35] An additional role for water is at the active site where a "catalytic water," used in peptide hydrolysis by the enzyme, is thought to hydrogen bond between Asp25 and Asp124.[32]

In this study we carry out long (greater than 70 ns) explicit solvent molecular dynamics (MD) simulations starting from a HIV-1 protease crystal structure obtained from a patient exhibiting multiple drug resistance[29] and, as a control, from a wild type (WT) apo protease crystal structure. Overall, the WT and MDR proteases ultimately deviate from their respective crystal structures to a similar extent. However, the WT exhibits a more localized structural change than the MDR that begins around 25 ns after initiation of the simulation. This WT "transition," which occurred from ~25–35 ns, involves a major motion of the flaps that results in an open form of the enzyme. The MDR mutant alters its overall configuration from the crystal structure very quickly relative to the

DOI 10.1002/prot

WT, while its flaps for the most part remain in the semi-closed form. The differing natures of the motions of the WT and MDR mutant in the flap regions are dissected with the use of a principal component analysis (PCA) method. Much of the fluctuations in both forms arise from fast flap curling motions, as was found in previous simulations[12,26] and NMR studies.[11,15] Our attention is mainly focused on the slower (on the MD time scale) and more collective motions that PCA is designed to pick up. The PCA does show that the transition behavior of the WT is dominated by a coherent motion of the flaps. By defining a triangular region whose sides connect the flaps to the catalytic site and the two flap tips we find a correlated expansion of the triangle that may be designed to entrap substrate for the WT. The corresponding MDR triangle fluctuates to a much smaller extent and does so in an uncorrelated manner. These contrasting features may suggest that active site expansion is more facile (takes place on a faster time scale) in the WT than in the MDR mutant, and supports the suggestion that conformational flexibility is important to catalytic activity. The use of explicit solvent and the relatively long simulation time permits exploration of the possibility of water diffusion into the active site. We find that water molecules do enter the active site and one water molecule will hydrogen bond, typically, to both catalytic aspartates with a distribution of residence times on the nanosecond time scale.

METHODS

Structural models

The wild-type crystal structure (1hhp) was obtained as a monomer[36] and imaged about its (x, y, z) twofold symmetry axis to generate the active dimer. The MDR mutant (1RPI) crystal structure was based on enzyme obtained from a patient who had received long-term drug therapy[29] with the additional mutation of Asp25 to Asn (D25N) at the active site (and similarly for the other monomer) to prevent auto-proteolysis. The WT and MDR sequences differ by the MDR-specific mutations: L10I, M36V, S37N, M46L, I54V, I62V, L63P A71V, I84V, L90M, and the additional residue mutation at the catalytic site D25N, and analogous mutations for the other monomer. The replacement of Asn by Asp was carried out with the MOE[37] software package. When these two structures (WT and MDR) had their main chain atoms superimposed, the root mean square deviation (RMSD) was 1.06 Å. To make a proper comparison between the MDR and WT differences, four structures, indicated by their pdb-code designations and catalytic residues, 1hhp(D25), 1hhp(D25N), 1RPI(N25D), and 1RPI(D25N) were utilized in our simulations. The data presented in the following are for 1hhp(D25), the WT with aspartates in the active site, and for 1RPI(N25D), the MDR where the asparagines were computationally replaced by aspartates in the active sites. The 70 ns data for the other combinations,WT-1hhp(D25N) and MDR-1RPI(D25N), that we ran are basically identical in their trajectories to the WT −1hhp(D25) and MDR (1RPI(N25D) pair, indicating that the results are not sensitive to the mutation of the catalytic aspartates to asparagines, or vice versa.

These additional runs were carried out in part to minimize the possibility that our results were a consequence of differing initial conditions arising from the different crystal structures. One way to test this and verify that the differing results of the WT and MDR mutant trajectories were not a direct consequence of the D25N mutation of the MDR enzyme is to mutate the WT to the D25N form and the MDR to the N25D form computationally and subject these two latter mutants to the same length of simulation. The behaviors reported in this paper for WT (D25) and MDR (N25D) were consistent with those exhibited by the WT (D25N) and MDR (D25N), illustrating that changing the initial conditions has essentially no effect on the overall trajectories. Furthermore, the simulation time of ∼70 ns is very long for typical MD runs and if initial conditions were still influencing the results on the 10 s of ns time scale, it would call into question the validity of many MD simulations.

Molecular dynamics

The MD trajectories were generated with the AMBER 7[38] package. The starting structures of HIV-1 protease (using any of the four structures) were loaded into the Leap module[39] with ∼5000 explicit water molecules (TIP3) introduced for the WT 1hhp(D25) and 8000 waters for 1hhp(D25N). Crystallographic waters were not included. For the MDR protease, ∼8000 waters were used for the 1RPI(N25D) and 1RPI(D25N) simulations. To achieve electroneutrality for the system, 6 Cl^- ions were added to the WT and MDR HIV (D25) species, while 4 Cl^- ions were added to the proteases containing the D25N mutation. In all simulations, the temperature was kept constant at 300 K with a Berendsen thermostat.[40] The particle mesh Ewald method[41] was used to treat long-range Coulombic interactions and the simulations performed using the SANDER module.[38] The ionization states of the residues were set appropriate to pH 7 with all histidines assumed neutral. The SHAKE algorithm was used to constrain bond lengths involving hydrogens, permitting a time step of 2 fs.

The protein and water were first run at constant number and pressure while the temperature was ramped from 100 to 300 K over ∼6 ps, to adjust the density to ∼1 g/ml, and then switched to the NVT ensemble for the dura-

tion of the simulations. The enzyme constructs were started with and without initial harmonic restraints (with relaxing the restraints from 15 to 0 kcal/(mol Å^2) over a 40 ps time period) on the whole system. No differences were observed in energy or structure in the initial behavior of the system.

In a simulation of WT HIV protease, Meagher and Carlson[14] found a difficulty with the simulation start up. There was rapid (~100 ps scale) flap motion that was traced to a deficiency of waters in the flap regions caused by the AMBER scheme of water deletion around a protein. They were able to cure this problem by a variety of methods including restraining the protein for a while to permit waters to diffuse into the cavity spanned by the flaps and the catalytic aspartates. In our simulations, we did not observe conformational changes of the flaps on this time scale. The AMBER protocol for solvating a solute uses a water box with lower than normal density, and then relies on a (short) fixed pressure simulation to adjust to normal density. In doing so, there can be pockets of vacuum/low density water that need to be eliminated. In our simulation of the WT there were initially ~25 waters inside the cavity. When the protein was heated to 300 K, and run for an additional 300–400 ps, apparently sufficient waters flowed into the cavity to prevent the collapse found by Meager and Carlson.[14]

Principal component analysis

In PCA[42–44] the covariance matrix $\sigma_{ij} = < \delta\alpha_i \delta\alpha_j >$ of the atom fluctuations $\delta\alpha_i$ from their trajectory-averaged $< \ldots >$ values, where $\delta\alpha_i(t) = \alpha_i(t) - < \alpha_i(t) >$ and $\alpha_i = \{x_i(t), y_i(t), z_i(t)\}$ denotes the Cartesian components of the ith atom, is diagonalized to produce the (orthonormal) eigenvectors $\mathbf{m}_i$ of the covariance matrix $\boldsymbol{\sigma}$ and the corresponding eigenvalues λ_i^2. The configuration point $\mathbf{r}^{3N}(t) = (x_1(t), y_1(t), \ldots, z_N(t))^T$ is decomposed as

$$\mathbf{r}^{3N}(t) = \sum_{i=1}^{3N} (\mathbf{r}^{3N}(t) \cdot \mathbf{m}_i)\mathbf{m}_i = \sum_{i=1}^{3N} p_i(t)\mathbf{m}_i \qquad (1)$$

where $p_i(t)$ is the trajectory projected in the direction of the ith eigenvector (mode). In the rotated 3N-dimensional Cartesian coordinate basis defined by the $\mathbf{m}_i$ $(i = 1, 2, \ldots, 3N)$ basis, the largest eigenvalue captures the largest fraction of the root mean square fluctuation (RMSF), the second largest the next largest fraction of the RMSF, etc of the trajectory data. Ordering the eigenvalues from large to small leads, in favorable cases, to a small set of modes that capture most of the protein's fluctuation. PCA is not restricted to harmonic motions; it can describe collective transitions between structures that differ greatly.

The contribution of atom j to the ith mode's fluctuation is obtained as $|\mathbf{m}_i^j| = \sqrt{(m_i^{jx})^2 + (m_i^{jy})^2 + (m_i^{jz})^2} \equiv \text{Component}_i^j$. The total RMSF^2 can be decomposed as

$$\begin{aligned} \text{RMSF}^2 &= \sum_i \lambda_i^2 = \sum_i \lambda_i^2 \mathbf{m}_i\, \mathbf{m}_i \\ &= \sum_i \sum_j \lambda_i^2 (m_i^{jx} m_i^{jx} + m_i^{jy} m_i^{jy} + m_i^{jz} m_i^{jz}) \\ &= \sum_i \sum_j (\lambda_i \text{Component}_i^j)^2 \equiv \sum_i \sum_j (R\text{-Component}_i^j)^2 \end{aligned} \qquad (2)$$

The product $\lambda_i \text{Component}_i^j \equiv R\text{-Component}_i^j \equiv R_i^j$ is the contribution of atom j in mode i to the total fluctuation of the protein. Use of R_i^j makes it possible to compare the importance of an atom across different modes; thus, we have termed it the relative contribution or R-Component. The time evolution of the ith mode is given by $p_i(t)$ as introduced in Eq. (1). If a particular $p_i(t)$ (or small set of $p_i(t)$) mirrors a significant motion that is implicit in the trajectory, then examination of the corresponding R_i^j will indicate which atoms contribute most to this motion.

Data analysis

The program Analyzer[45] was used for most of the analysis of the MD trajectories. Root-mean-square deviations (RMSD) from crystal structures and root-mean-square fluctuations (RMSF) from trajectory-averaged structures, along with the various PCA-based measures discussed above were generated by Analyzer. Distance measurements over the trajectories were generated using the Ptraj module of AMBER.[38]

RESULTS

RMSD/RMSF

The CA atom RMSDs displayed in Figure 2 over the total simulation time indicates that the MDR structure deviates somewhat more from its crystal structure than the WT. The largest variations in the WT and MDR occur in the tips of the "flap" regions (residues 46–54 and 145–153 in monomer A and B, respectively). There is an asymmetry between the two monomers in the WT that is especially prominent in the flap region. The total CA RMSD as a function of time (Fig. 3) shows that the MDR enzyme deviates within a few ns from its crystal structure while the WT does not. Indeed, the WT protease exhibits very little deviation from its crystal structure for the first ~30 ns, and then there is a transition to a new state. After the WT transition, it and the MDR have

 DOI 10.1002/prot

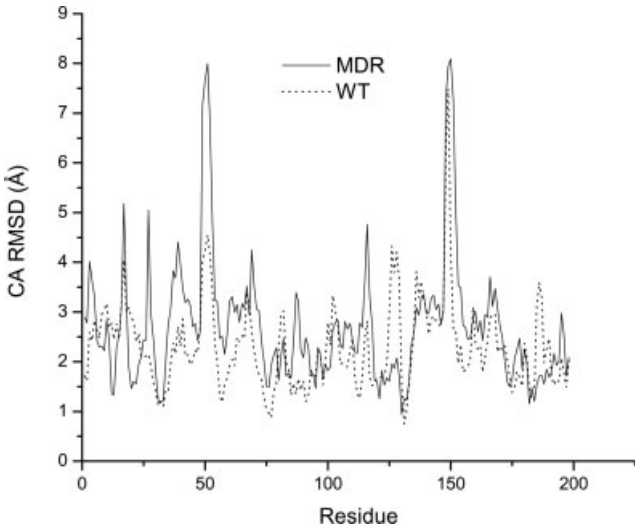

Figure 2

RMSD from the crystal structure over the whole MD simulation of backbone CAs. Notice the mainly greater deviation of the MDR (solid line) flap regions than that of the WT (dotted line).

similar total CA RMSD values. The total CA RMSD versus time of the MDR mutant excluding the flap tips (residues 46–54 monomer A and residues 145–153 monomer B) mirrors that displayed in Figure 3, with the differences concentrated in first few 100 ps (data not shown). Thus, the initial deviation from the x-ray structure cannot be ascribed to a large flap tip motion; the motions responsible for the deviation are spread throughout the protein. The CA RMSFs of the WT (Fig. 4) are mainly larger than those of the MDR. The largest RMSFs are found in the tips of the flap regions in both proteases. In Figure 4, each monomer configuration was separately fit (superposed) to its corresponding reference monomer. A similar result is found by superposition on the respective dimers.

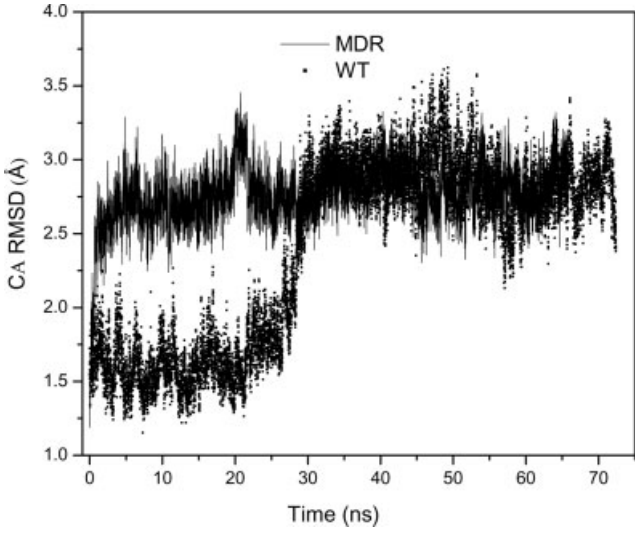

Figure 3

RMSD of the backbone CAs from the crystal structure versus time. The MDR crystal structure (solid line) shows immediate movement away from its initial structure. However, there is a later "transition" of the WT (dotted line) from the crystal structure during an ~10 ns interval, 25–35 ns.

Distance measurements

Figure 5 displays the time evolution of the distance between the catalytic Asp25 CB and the flap tip Ile50 CA

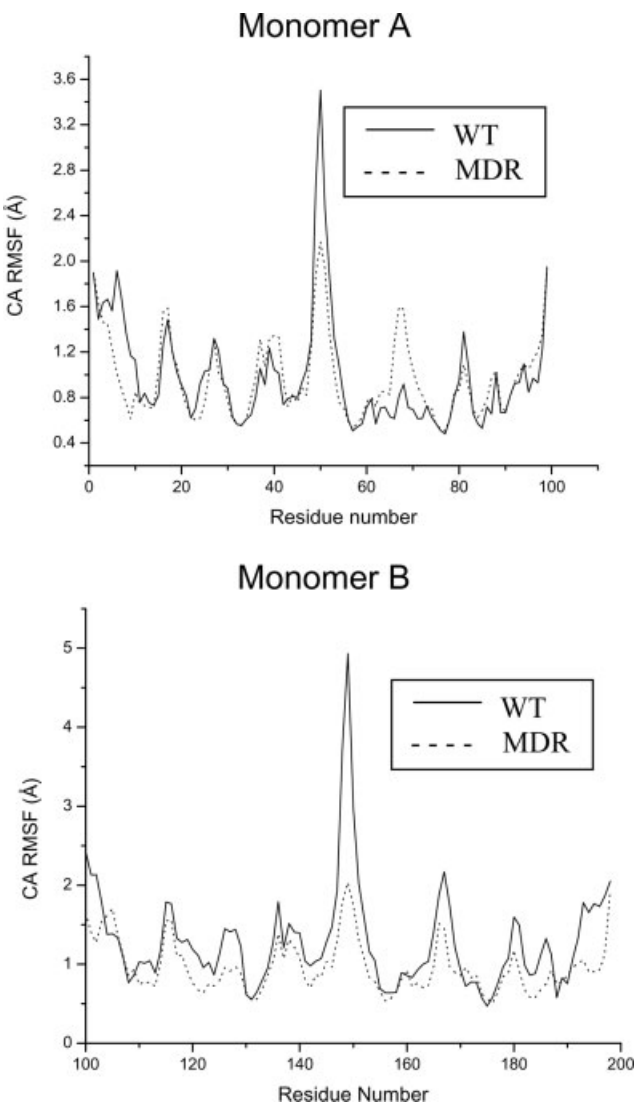

Figure 4

RMSF of the backbone CAs over the entire simulation of the WT (solid line) and MDR (dotted line) separated into their monomers.

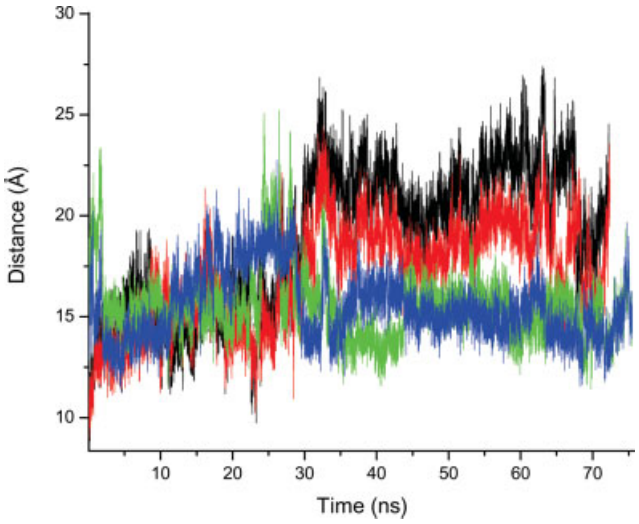

Figure 5

Distance of the flap tips to catalytic aspartates measured from I50 CA to D25 CB for monomer A (I149 to D124 for monomer B): WT monomer A (red), B (black); MDR monomer A (green), B (blue). Both monomers of the WT show a large increase in the measured distance over the same time interval as the "transition" interval identified in Figure 3. Conversely, the MDR atom positions move closer together.

for each monomer. If the semi-open form of the enzyme is indicated by this distance being ~15.8 Å[26] then the MDR mutant monomers exist predominantly in this form for a few ns in the time interval 0–30 ns. During the same time interval, the WT samples this distance less frequently, staying in a more "closed-like" conformation than does the MDR protease. Histograms of the data (Fig. 5) are shown in Figure 6. The average distance of the WT monomers are ~15 Å, while those of the MDR mutant consistently sample regions that are >16 Å, over the 0–30 ns time interval. From ~25–35 ns the significant structural transition of the WT is evident in the RMSD data of Figure 3 and is reflected in the increase in the distance of the catalytic aspartates to the flap tips of monomer A and B, as shown in Figure 5. This structural transition is also observed in the histogram peaks that have shifted to the right indicating a higher probability of a more open form for monomer A and monomer B [Fig. 6(A)]. In the MDR mutant, the 0–30 ns histograms exhibit bi-model distributions that reflect a sampling of semi-open to open distances. The 30–72 ns histograms indicate that the MDR monomers adopt a more closed configuration with a narrower distribution of catalytic aspartate to flap-tip distance [Fig. 6(B)].

The distances between the flap tips and their respective catalytic aspartates, $d_{25–50}$ and $d_{124–149}$, and the flap tip to flap tip distance $d_{50–149}$ can be viewed as forming a triangle (by merging the two catalytic aspartates) that can be used as a proxy for the space available to insert substrate. Figure 7 displays 3D plots, along with their 2D projections, of the dimensions of this triangle for the

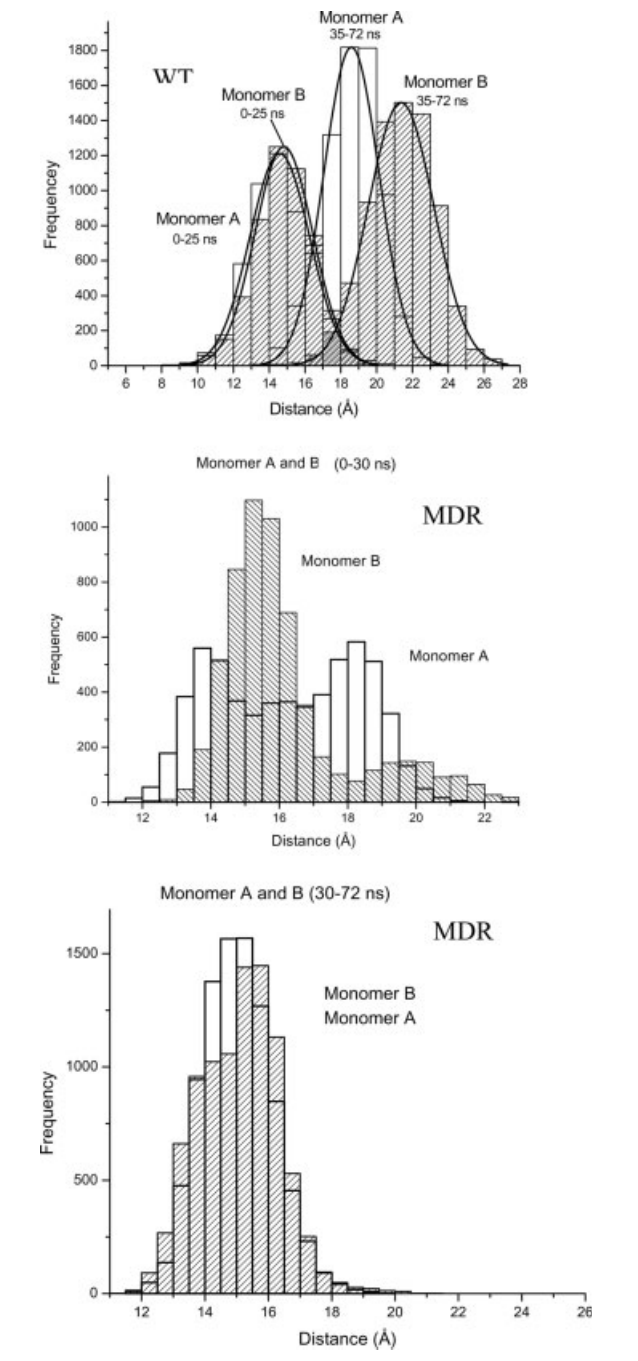

Figure 6

Histograms of the distance between the flap tip (I50 (I149) monomer A (B)) and the catalytic residue (D25 (D124) monomer A (B)). WT flaps (top panel) are initially similar (0–25 ns) and are in an open form with different average distances (35–72 ns). The MDR (0–30 ns, middle panel) distances show a bi-modal distribution while during the later period (30–72 ns, bottom panel) they adopt a more or less symmetrical closed-like form.

DOI 10.1002/prot

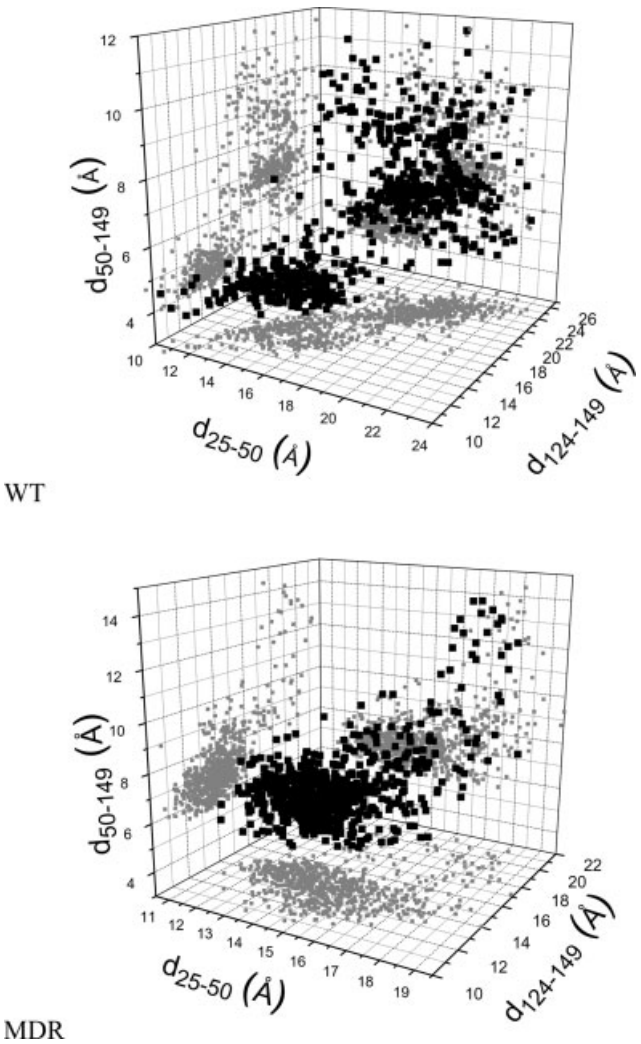

Figure 7

3D plots and their 2D projections from trajectory snapshots of the triangle formed by the flap tip to catalytic aspartate distances, d_{25-50}, $d_{124-149}$, and the flap tip to flap tip distance d_{25-149}. WT (top panel) showing two states with one consisting of small area triangles and the other of larger area triangles, illustrating a more closed-like form moving to a more open one. MDR mutant (bottom panel) showing one state throughout the entire simulation.

WT [Fig. 7(A)] and MDR [Fig. 7(B)] simulation data. In the WT there are two states evident in the 3D triangle plot. The triangle area goes from around 35 to 55 Å^2 defining, respectively, two clusters corresponding to a small and large triangle. A large part of the transition behavior evident in the RMSD data displayed in Figure 3 can be accounted for by the behavior of this triangle. The transition between small and large triangle occurs by a correlated expansion, where all three distances increase in a coherent manner, as is clear from the 2D projections. After the transition, the averages of the flap tip to respective catalytic aspartate distances do differ by about 3 Å, so the larger triangle state is not isosceles.

In the MDR protease, the 3D triangle plot and its corresponding 2D projections [Fig. 7(B)] show no evidence for two-state behavior (in agreement with the RMSD versus time data displayed in Fig. 3). For the bulk of the data, the 2D projection plots show a lack of correlation in the respective pairs of distances excursions. For the rare excursions where the flap tip to flap tip distance becomes large, the flap tip to catalytic aspartate distances (separately) do follow. Thus, the mutant triangle (of approximate dimension 45 Å^2) has its sides mainly fluctuating in an uncorrelated fashion.

Principal component analysis

A PCA of the WT and MDR HIV trajectories was carried out. The data are summarized in Table I based on an analysis of the dimer (D) and the separate monomers (A and B). Note that the superpositions that are used to process the trajectory data are different for the three cases D, A and B. In addition to the total trajectory, PCA on the WT was carried out in three intervals, 0–25, 25–35, and 35–72 ns, and we will refer to the 25–35 ns interval as the transition interval because the WT transitions between two conformational states during this time period. The total RMSF^2 (from the CA atoms) is listed along with the percentages due to the first three PCA eigenvectors, which we shall refer to as Modes 1, 2, and 3.

Table I

Total Fluctuation and % Contributions From the First Three PCA Modes of WT and MDR HIV.

Time range (ns)	WT D[a]	WT A[b]	WT B[c]	MDR D[a]	MDR A[b]	MDR B[c]
0–72						
RMSF^2 (Å^2)	2155	485	809	1191	428	417
Mode 1 (%)	48	55	51	25	23.5	22.3
Mode 2 (%)	12	3.7	8	14	16.5	12.5
Mode 3 (%)	5	2.9	6	7	5.6	8.7
0–25						
RMSF^2 (Å^2)	1282	450	427	1141		
Mode 1 (%)	27.2	30.0	21.5	36.0		
Mode 2 (%)	21.0	16.0	18.3	13.5		
Mode 3 (%)	8.0	6.5	9.0	5.5		
35–72						
RMSF^2 (Å^2)	987	281	390	823		
Mode 1 (%)	23.0	17.4	17.3	18.0		
Mode 2 (%)	11.0	9.7	13.3	12.0		
Mode 3 (%)	9.5	4.8	8.7	6.7		
25–35						
RMSF^2 (Å^2)		362.85	562.87			
Mode 1 (%)		31.5	47.0			
Mode 2 (%)		16.6	7.8			
Mode 3 (%)		6.7	5.7			

[a]Superposition of frames carried out on dimer.
[b]Superposition of frames carried out on monomer A.
[c]Superposition of frames carried out on monomer B.

The WT RMSF^2 over the 0–72 ns interval is larger than that of the MDR but the RMSF^{2}s are comparable over the 0–25 and 35–72 ns intervals. The differences in this regard are concentrated in the 25–35 ns transition interval. The WT has a greater variation in its first three modes than that of the MDR mutant. Indeed, 60% of the WT RMSF^2 is contained in the first two modes, while the same percentage requires seven modes in the MDR mutant. The MDR monomers exhibit comparable behavior while the WT monomers are different in scale, the difference more evident in the transition interval, and in the 35–72 ns interval. In agreement with the WT monomer RMSFs in Figure 4 and flap tip to catalytic aspartate distances in Figure 5, it is evident that the WT monomer B is undergoing a larger motion than A.

To trace these behaviors to atom displacements, the RMSFs of each CA corresponding to the trajectories of the first three modes were obtained. In each time interval and for each mode, the flap tip region is prominent. In the PCA using the total simulation time the WT monomers appear quite similar, but in the interval data the transition time RMSFs are mainly sharper, especially for monomer B. The data for the transition interval is displayed in Figure 8, using the R-components defined in Eq. (2) that permits comparison of atom RMSFs among different modes. (The data over the total time for Mode 1 is very similar to Figure 8 for the transition interval.) Mode 1 is dominated by the flap tip region and this is more so in monomer B. This mode also shows (especially in monomer B) movement in residues 64 through 69 which form a β-turn after the flap region at the base of the enzyme. This indicates that the latter region, along with other noticeable regions, show some flexibility and moves in a concerted motion with the flap region.

For Mode 1 in the other time intervals, (data not shown) monomer A is also dominated by the tip region but monomer B also has other prominent peaks. The percentages for Modes 2 and 3 are rather small and their motions, aside from always having a component from around the flap tip, does involve significant displacements of quite a few atoms. The modes in a PCA are of course collective properties, and the behavior exhibited by Mode 1, with its rather strong concentration around the flap tip is evidence of a more local motion. Comparing Modes 1 and 2 in Figure 8 shows that the proportion of tip motion is larger in Mode 1, indicating that a more local motion is captured in Mode 1.

That the atom motions for Mode 1 of the WT have a large contribution around the tip holds for the three time intervals (0–25, 25–35, and 35–72). Yet, there must be a distinction between the motions in the transition and non-transition intervals. From RMSF measures it is not clear if a (random) oscillatory motion (which we use as a term to characterize flap tip fluctuations) or a transition between two conformations is occurring. Therefore, we examine the $p_i(t)$ $(i = 1–3)$, which are the pro-

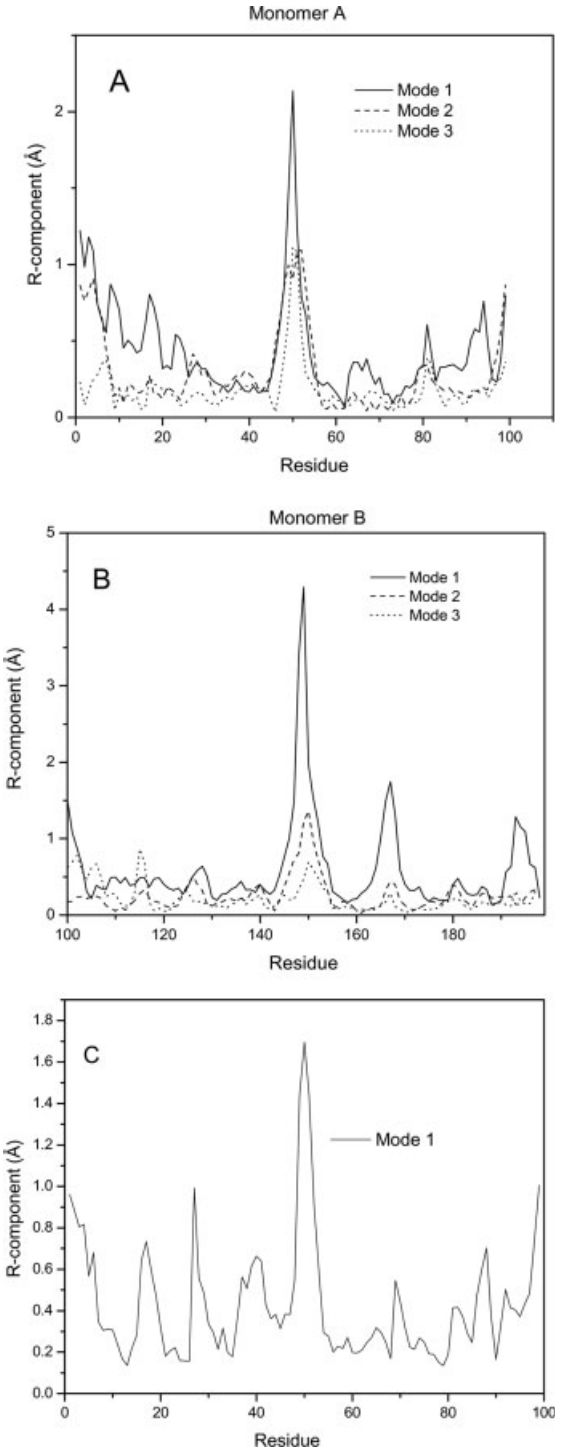

Figure 8

*CA RMSFs for dominant PCA modes of the WT and MDR over the transition interval, 25–35 ns. (**A**) and (**B**) Monomer A and B respectively of the WT showing mode one (line), two (dash) and three (dots). The dominance of the flap (res 49–54) motion is evident, especially in monomer B. (**C**) A similar RMSF pattern is found in the MDR mutant (showing monomer A; monomer B not shown) indicating that flap motion is prominent in both enzymes.*

DOI 10.1002/prot

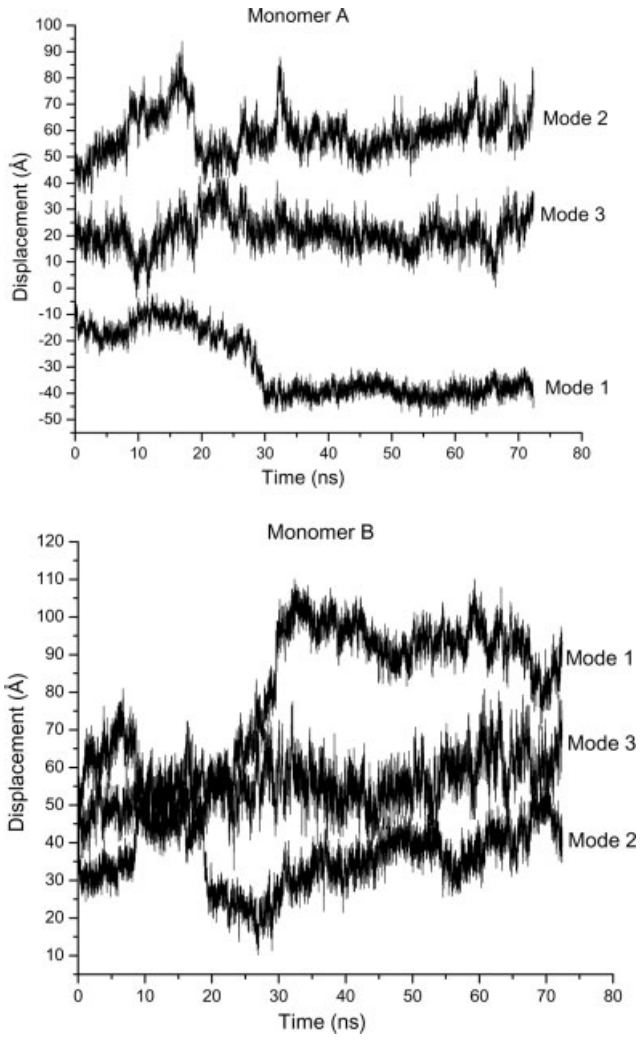

Figure 9

The projections of the trajectory onto the first three modes for the WT monomer A and B. Only Mode 1 reflects the transition behavior (25–35 ns).

jections of the trajectory onto the first three PCA eigenvectors. These projections, displayed in Figure 9, show that only Mode 1 describes the transition behavior, and the effect is more dramatic in monomer B. Thus, while Modes 2 and 3 have strong contributions from the flap tip region, they are not describing the transition between states. Only Mode 1 incorporates this behavior. That Mode 1 for monomer B has a more dramatic transition is consistent with the mode percentages in Table I and the relatively larger tip peak in Figure 8. In the other time intervals, the Mode 1 monomer B and A tip peaks are comparable. Thus, over the entire simulation, there is an oscillatory motion of the flap tip region, and the transition behavior that corresponds to the flap tip moving between two states is superimposed on this oscillatory motion.

In monitoring the curling behavior [Fig. 10(A)] of the WT, it was noticed, as with Perryman *et al.*[26] that the flaps sample different angles on two time scales; one on the ps and the other on the ns time scale. We also observed during the transition time a substantial alteration in the angles whereby both monomers become synchronized. This is consistent with the idea that the curling of the tips triggers the opening of the entire flap region.[23,26,46] In the MDR enzyme, the flaps never consistently synchronize in their behavior and hence never achieve an "open" structure [Fig. 10(B)].

The percentage contributions of Mode 1 are around 25% for the MDR dimer and monomers. Thus, Mode 1 is not as important to the MDR as the WT, most likely due to the large influence of the transition behavior on the WT Mode 1. The Mode 1 MDR pattern of CA RMSF versus residue based on monomer superpositions is similar in pattern to the WT Mode 1 monomer A

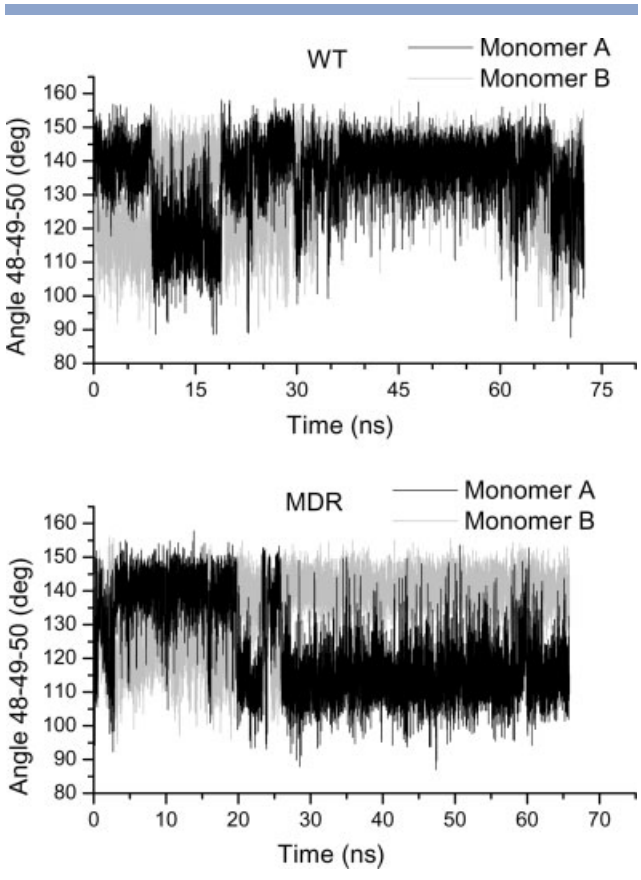

Figure 10

*Flap curling, defined by the angle formed from the three CAs of G48-G49-I50 (G147-G148-I149) monomer A (monomer B), versus time. (**A**) WT shows monomer A (black) and monomer B (gray) exchanging angles initially, but synchronizing their behavior at ~35 ns with both monomers having a less bent structure until 60 ns. (**B**) MDR shows monomer A (black) and B (gray) swapping angles for most of the simulation.*

[Fig. 8(C)]. This indicates that the flap tip residue oscillations are dominating Mode 1, and are the most important motion in the MDR. In the WT and MDR mutant, the dominant motion excluding the transition behavior of the WT that is identified by Mode 1 is the flap tip oscillation.

WT catalytic aspartates 25 and 124

The catalytic residues (Asp 25; Asp 124) sitting at the bottom of the active site have their OD1 oxygens within ~3 Å of each other upon dimerization. The carboxylates of both aspartates (the two carboxylate oxygens are denoted as OD1 and OD2) are hydrogen bond acceptors for waters. The approach of Asp25 and Asp124 results in the scaffolding upon which a water molecule required for catalysis can bind.[31,47,48] During the simulation, water molecules migrated to the catalytic residues Asp25 and Asp124 to form hydrogen bonds, and would subsequently depart, with different residence lifetimes. When bound, a water molecule bridges Asp25 and Asp124 by hydrogen bonding to both residues. In all cases, water occupied the catalytic site on the ns time scale. Some of the time, a water molecule occupied this catalytic site for up to ~6 ns (Fig. 11). In this latter instance, Asp25 OD1 maintains hydrogen bonding contact with WAT 2215 throughout the ~6 ns while Asp124 has its OD1 and OD2 exchange their hydrogen bonding positions over this same time interval. Contrary to the waters in WT HIV, water molecules at the active site in the separate simulation of the MDR with the asparagines from the crystal structure 1RPI(D25N) have on average much shorter dwell times. Indeed, throughout the MDR simulation the only durable hydrogen bonding at this site was between the OD1 oxygen of one monomer (D25N) to the other monomer's (D124N) ND2 nitrogen.

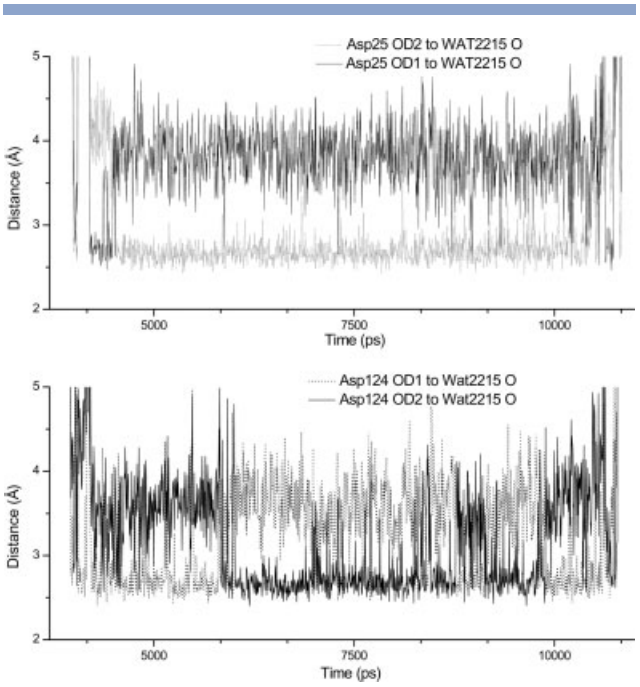

Figure 11

Catalytic water bridged between monomers. The aspartate carboxylate oxygens, labeled OD1 and OD2, are hydrogen bond acceptors for water. Top panel: the distance of OD1 (solid line) and OD2 (dotted line) of Asp25 to the oxygen of water 2215. There is no exchange between OD1 and OD2 for several ns. Bottom panel: OD1 (dashed line) and OD2 (solid line) of Asp124. There are multiple exchanges between the oxygens that bridge the catalytic water. This was found to be typical throughout the entire simulation.

DISCUSSION

The HIV protease simulations were carried out without a ligand because we were most interested in contrasting the WT and MDR mutant apo protease conformational fluctuations. The great number of HIV protease crystal structures obtained and simulations preformed with a variety of ligands show that the binding cavity can take on many different shapes, and corresponds to volumes that can differ by a factor of two. Consistent with this, our data shows substantial differences associated with the separate proteins where the plasticity is mainly because of a consequence of the flexibility of the flap regions, with their high glycine content.[12]

To validate the simulation results on the WT 1hhp(D25) with the catalytic aspartates and the MDR 1RPI(N25D), 70 ns simulations were also carried out on the MDR mutant 1RPI(D25N) and the WT 1hhp(D25N) to see if the major effect was from the presence of active site asparagines. The results show that this is not the case. The data for these latter simulations (not shown) are essentially the same as that presented here, indicating that the WT transition behavior and lack of this feature in the MDR mutant are not affected by the replacement of the two (charged) aspartates by two (neutral) asparagines. This replacement, of course, creates different initial conditions for both the WT and the MDR HIV protease that is much more pronounced than starting different trajectories by using different velocity distributions, and provides further evidence that there is a real distinction between the WT and MDR varieties of the protease. Furthermore, the long durations of the simulations should be beyond the influence of initial conditions, such as differing initial velocities, on the trajectories.

The distances between the catalytic Asp25 to the flap tip residue Ile50 displayed in Figure 5 show that the MDR mutant (for the majority of the simulation) and the WT initially are in what has been referred to as a semi-open form (see below) for the first ~25 ns, which is thought to be a favorable structure[11,26,27,49] based on previous simulations and NMR studies. However, the

DOI 10.1002/prot

WT, starting around 25 ns (Fig. 5), extends itself to an "open" form over 10 ns, after which it remains open for the rest of the simulation, which is consistent with the RMSD data (Fig. 3). The histograms (Fig. 6) of the distance data of Figure 5 illustrate that both WT monomers undergo a transition to states with larger average flap-tip to catalytic residue distances than before the transition with monomer A's average distance at ~18 Å and monomer B's at ~21 Å. In contrast, the monomers of the MDR mutant have their average distance around 16 Å through the first ~30 ns and slightly contracted to around 15 Å for the interval 35–72.

NMR studies indicate that the predominant form of WT HIV protease is the semi-open structure with the flap tip residues (46–54) moving on a nanosecond time scale.[11,50] In addition, apo protease free-energy simulations[49] point to the semi-open form as more stable than the closed form due to entropic effects in the flap region. However, in simulations of the solvated apo enzyme without any constraints, WT HIV has been observed to go from the semi-open to a fully open structure on the nanosecond time scale, exhibiting asymmetric flap behavior.[12] On the basis of a series of 3 ns simulations of WT HIV, Meagher and Carlson[14] suggested that the semi-open form would be stabilized by crystalline contacts, and that the loss of these contacts in a solvated MD simulation would destabilize the semi-open conformation A long (42 ns) implicit solvent simulation[27] of a WT HIV protease, with its ligand removed, had a definite preference for the semi-open form but sampled the closed, semi-open and open conformations. Our studies do show that this semi-open form is one of at least two stable forms found in our 70 ns simulation. The second, stable open configuration occurred after the first ~30 ns. The MD simulation[12] that found opening on a scale of 1 ns was contrasted with NMR experiments where flap opening was assigned to the ms-μs time scale.[11,50] The NMR structure may be more open than what we find on the 30 ns time scale. However, it is difficult to compare the forms of the open states because the NMR analysis provides a time scale, and the information that there is a significant structural change, but cannot provide an atomistic structure.

The MDR mutant containing multiple mutations (in the active and other sites), including several possibly acting as "compensatory mutations" (e.g. M46L; see Introduction), adopts a semi-open to closed forms during the simulation, and does not exhibit motions that lead to large flap openings. This behavior of the flaps adopting a closed-like form has been observed before with the non-active site mutation M46I, which induces indinavir resistance.[51] MD (vacuum) studies of this apo HIV M46I mutant showed that it retains, over the simulation time investigated, a closed state in comparison to the apo WT protease under the same conditions of an external force used to drive the protease core residues from a closed conformation to one in a semi-open structure.[52] Using explicit water and longer simulation times, it was shown that the flap region of ligand-bound WT HIV exhibited greater flexibility than the ligand-bound mutant M46I in the same region.[23] Indeed, several crystal structures of HIV proteases containing certain mutations exhibit lower flexibility, as indicated by their smaller B factor values.[22,23,53,54] In another study using crystallographic temperature factor comparisons between the flap mutant (G48H) and WT HIV, it was found that the flap regions were more rigid in their mobility than the WT enzyme.[55] This connection between the reduced flap mobility and the enzyme's ability to bind inhibitor efficiently has been suggested in several studies.[23,56,57] In our study, the *in vivo* mutated sites leading to the MDR species showed no significant fluctuations (RMSFs) and thus the difference in the motion between the WT and MDR are an accumulative (coupled) event.

The PCA of the WT and MDR was carried out to see if large amplitude modes exist and, if so, to identify the nature of the motions to which they correspond. With the known distinction between the mobile flap regions and the more rigid core of the remainder of the protease, a PCA analysis should provide a good separation into a few important modes and a large number of small, essentially Gaussian fluctuation modes. There is, indeed, good separation of the overall mean square fluctuation, with the first two modes contributing 60% of the total $RMSF^2$ for the WT. To obtain the same percentage requires seven modes in the MDR mutant that, while still a small number of modes, does indicate a significant difference between the WT and MDR proteases. The MDR protease motion is less coherent than that of the WT.

For the WT over the entire simulation time, Mode 1 contributes ~50% to the total $RMSF^2$ whether based on dimer or monomer superposition (Table I). Note the strong similarity between the CA RMSFs of Mode 1 (Fig. 8) and those based on the trajectory atom displacements for 25–35 ns (Fig. 4). (The agreement is even closer for the RMSFs when evaluated for the entire trajectory). The atom displacements that contribute the most to Mode 1 are concentrated in the flap tips. Projecting the trajectory onto the first three eigenvectors (Fig. 9) does show that it is Mode 1 that carries not only the information on the flap tip oscillations but also describes the transition behavior. Carrying out separate PCAs on these different time intervals (pretransition 0–25 ns (data not shown), transition 25–35 ns (Fig. 8) and post-transition times 35–72 ns (data not shown)) also confirms that Mode 1 has an important contribution in each interval from flap tip motions. The picture that emerges from the mode analysis is of rapid and persistent flap tip oscillation that has superimposed on it the slower, large-scale change in conformation that takes place in the transition interval. The atom motions corresponding to Mode 1 in the transition and a non-transition interval are indicated

in Figure 12(A,B). Note that in the *i*th PCA mode the corresponding atom displacements are given by $\mathbf{r}_i^{3N}(t) = p_i(t)\mathbf{m}_i$, [cf. Eq. (1)], so that all the atoms move with the same time dependence. The arrows drawn in Figure 12(A) (the WT) indicate that the coherent mode motion counterbalances the flap tip and the residue 64–69 regions.

As stated, the MDR mutant does not exhibit the transition behavior found in the WT that leads to the open configuration. That might suggest that the first few modes are not as important for the MDR as for the WT, which is correct in terms of percentage contributions to the total RMSF[2]. Nevertheless, Mode 1 of the MDR is still a faithful descriptor of the important flap motion, as a comparison of the RMSFs in Figure 4 and the data for MDR Mode 1 shown in Figure 8(C). These similarities in flap patterns between WT HIV and MDR illustrate the importance of flap tip motion, though there are certainly differences for other residue regions. The data indicate that flap tip residue oscillations dominate Mode 1, and are the most important motion in the MDR. Thus, the key motion of flap tip oscillation is common to the MDR and WT proteases. The differences between them are associated with the much longer time scale motions associated with the WT transition behavior.

The PCA identifies the key motions of flap tip oscillation and, in the WT, a conformational transition with displacements concentrated in the flap region. The triangle analysis summarized by Figure 7(A) suggests that there is a coherent expansion of this triangle that may provide the fluctuations to, when open, trap substrate and, when closed, aid in forming the catalytically active geometry. Not only do the $d_{25–50}$ and $d_{124–149}$ distances increase in concert, but also so does the $d_{25–149}$ distance. This conclusion is based on the strong correlation between the flap tip and respective catalytic aspartate distances, $d_{25–50}$ and $d_{124–149}$, as well as the correlation with the $d_{25–149}$ distance that is evident by projecting the 3D data onto the three 2D planes. There is a tendency for the flap tip to flap tip distance $d_{50–149}$ to remain around 4.5 Å while the $d_{25–50}$ and $d_{124–149}$ distances increase to around 17 Å and, for further increase in the $d_{25–50}$ and $d_{124–149}$ distances, the $d_{25–149}$ distance transitions to around 7 Å. Thus, it appears that the (correlated) increase of flap tip to catalytic aspartate distances permits a transition in the flap tip to flap tip distance. In contrast to this coherent expansion of the WT triangle, not only does the MDR exhibit a more compact structure, but also the sides of the triangle do not exhibit correlated motion for most of the trajectory data. Only when there are unusually large distance excursions, which are concentrated in the shorter time data, is there a connection among these distances. Another manifestation of the correlated behavior in the WT is seen in Figure 10, where the flap angles of the WT synchronize their flap movement during the transition period, moving to a less bent (un-curled) structure. The un-curled geometry of both the flaps appears to occur only after the opening (increasing distance between I50 and I149) of the dimer.

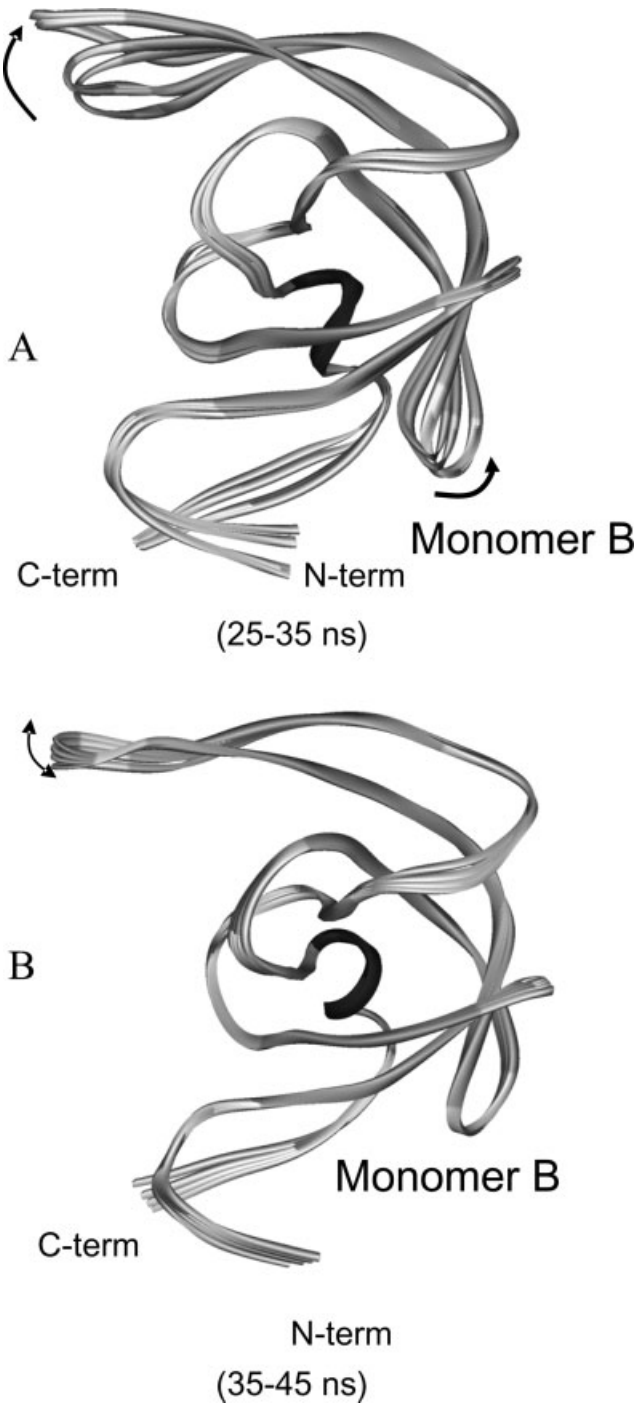

Figure 12

*Structural representation of mode one trajectories: (**A**) WT monomer B during the transition time (25–35 ns) with the arrow showing the directionality of the motion. (**B**) WT monomer B during the 35–45 ns time interval with the double arrow indicting the non-directionality of movement.*

DOI 10.1002/prot

This result is consistent with the proposition that the flap tips might be controlling the opening process for substrate entry.[15,24,26]

Water movement to the catalytic site during the simulation of the WT protease was investigated. Initially, no water was present near the catalytic site, but eventually a water molecule consistently bridged the two catalytic aspartates by hydrogen bonding to them. The lifetime of these waters varies from around 1 ns to several ns (4–7 ns). In Figure 11, one such situation is shown where the Asp25 OD2 is in hydrogen bonding contact with W2215 for ~6 ns while OD1 and OD2 of Asp 124 exchange with W2215. No correlation between the carboxyl group rotations (measuring the dihedral given by the backbone N, CA, CB and OD2 between CA and CB of either Asp25 or Asp124) and the exchange of water molecules was found. Similar water behavior was found for the MDR 1RPI(N25D) protease (data not shown). Slower exchange rate water molecules that bridge the catalytic aspartates could support the hydrolysis of the peptide bonds. In contrast, the MDR mutant 1RPI(D25N) exhibits mobile waters having no active site residence lifetimes greater than 1 ns and with no water bridging between the "catalytic" residues. Instead of two charged aspartates acting as acceptors for forming hydrogen bonds to water, the asparagines provide the opportunity for the observed consistent hydrogen bonding between the OD1 of one monomer and the ND2 of the other monomer. In terms of a reaction mechanism, it is thought that the aspartates in the HIV catalytic site share one proton, with the net −1 charge delocalized over both carboxylates. When substrate binds, it has been suggested that the aspartates are disrupted with one becoming protonated and the other negatively charged. Subsequently, the charged aspartate deprotonates a water molecule and then the hydroxyl nucleophile attacks the backbone carboxyl of the substrate peptide.[58–60]

CONCLUDING REMARKS

The MDR protease, with its mutations indicated in Figure 1(B), is resistant to therapeutic drugs, but still maintains activity with its natural substrate. To gain insight into why these mutations in the MDR protease confer such resistance, long (~70 ns) MD simulations in explicit solvent were performed on the MDR mutant and a WT protease to observe their structural fluctuations on a multi-nanosecond time scale.

Analysis of the entire trajectory shows that the flap tips are capable of rapid fluctuations that correspond to a curling motion. RMSF measures show that the flap tip regions are the most flexible parts of the WT and MDR proteases. The WT protease also exhibits a much slower motion that corresponds to opening of the flap tips. Investigation by PCA shows that there is dominant mode of motion that has major contributions from the flap regions for both proteases.

The WT protease undergoes a transition that mainly arises from a concerted motion of the flap tips relative to their catalytic residues and the relative motion of the two flap tips. The triangle formed by these residues opens up the active site from the initial semi-open to an open form, and the expansion takes place in a coherent manner. During this expansion, the flap tip geometry changes from a more curled to a less curled form, and that geometry persists for a long time after the transition. In contrast, the MDR protease remains in a more semi-closed configuration with uncorrelated fluctuations in the distances defining the triangle.

Understanding the mechanism of substrate/inhibitor specificity between the WT and MDR, and how this process depends on the flap behavior is challenging. One possible scenario that is consistent with the simulation results is based on the contrast between the long polypeptide chain substrate of HIV protease and its inhibitors that tend to be small molecules. If the polypeptide section to be cleaved has a pre-bound state with a part inside the protease and other portions in interaction with the surface around the attachment region, then one can envision this first step as initial attachment of the substrate to enzyme. The access of the polypeptide substrate to the interior depends on the flap movement of HIV, but it is positioned favorably to take advantage of the flap opening when it occurs. Once access to the interior of the protease is achieved, in a second step, the polypeptide can move into the active site and be positioned in a proper orientation to be cleaved. In this scenario, it would be easier for WT HIV than the MDR to complete the initial interaction of "jamming" the active site because of the larger fluctuations of the WT. But, once this initial binding has taken place, both the WT and MDR behave in a similar fashion with regard to binding to the active site. If this second step is rate limiting, then the WT and MDR bind the polypeptide similarly. Consequently, the larger flap fluctuations in the WT versus the MDR would not influence the polypeptide binding. For the inhibitor with the MDR protease, because the inhibitor is small, it might not be able to position itself on the enzyme to take advantage of the rare openings of the flap region, while with the WT, the inhibitor can more readily gain access. Therefore, for an inhibitor, in contrast to the polypeptide, the enhanced flap fluctuations in the WT lead to better inhibitor binding in the WT relative to the MDR. In summary, this scheme suggests that the substrate would out-compete the inhibitor in the MDR HIV, and that the MDR and WT would behave the same once true substrate is initially bound. This would explain the difference between a candidate inhibitor's ability to be an effective inhibitor of the WT, but not the MDR protease.

ACKNOWLEDGMENTS

A generous grant of computer time from the Michigan State University High Performance Computing Center is gratefully acknowledged.

REFERENCES

1. Kohl NE, Emini EA, Schleif WA, Davis LJ, Heimbach JC, Dixon RAF, Scolnick EM, Sigal IS. Active human immunodeficiency virus protease is required for viral infectivity. Proc Natl Acad Sci USA 1988;85:4686–4690.
2. Pechik IV, Gustchina AE, Andreeva NS, Fedorov AA. FEBS Lett 1989;247:118–122.
3. Perl LH, Taylor WR. A structural model for the retroviral proteases. Nature 1987;329:351–354.
4. Lapatto R, Blundell T, Hemmings A, Overington J, Wilderspin A, Wood S, Merson JR, Whittle PJ, Danley DE, Geoghegan KF, Hawrylik SJ, Lee SE, Scheld KG, Hobart PM. X-ray-analysis of HIV-1 proteinase at 2.7 a resolution confirms structural homology among retroviral enzymes. Nature 1989;342:299–302.
5. Navia MA, Fitzgerald PMD, Mckeever BM, Leu CT, Heimbach JC, Herber WK, Sigal IS, Darke PL, Springer JP. 3-Dimensional structure of aspartyl protease from human immunodeficiency virus HIV-1. Nature 1989;337:615–620.
6. Miller M, Jaskololski M, Rao JK, Leis J, Wlodawer A. Crystal structure of a retroviral protease relationship to aspartic protease family. Nature 1989;337:576–579.
7. Toh H, Ono M, Saigo K, Miyata T. Retroviral protease-like sequence in the yeast transposon Ty1. Nature 1985;315:691–692.
8. Wlodawer A, Erickson JW. Structure-based inhibitors of HIV-1 protease. Ann Rev Biochem 1993;62:543–585.
9. Gulnik S, Erickson J, Xie D. HIV protease: enzyme function and drug resistence. In: Litwack G, editor. Vitamins and hormones, Vol.58. San Diego, CA: Academic Press; 2000. pp 213–256.
10. Wlodawer A, Vondrasek J. Inhibitors of HIV-1 protease: a major success of structure-assisted drug design. Ann Rev Biophys Biomol Struct 1998;27:249–284.
11. Ishima R, Freedberg DI, Wang YX, Louis JM, Torchia DA. Flap opening and dimer-interface flexibility in the free and inhibitor-bound HIV protease, and their implications for function. Structure 1999;7:1047–1055.
12. Scott WRP, Schiffer CA. Curling of flap tips in HIV-1 protease as a mechanism for substrate entry and tolerance of drug resistance. Structure 2000;8:1259–1265.
13. Hamelberg D, McCammon JA. Fast peptidyl cis-trans isomerization within the flexible Gly-rich flaps of HIV-1 protease. J Am Chem Soc 2005;127:13778–13779.
14. Meagher KL, Carlson HA. Solvation influences flap collapse in HIV-1 protease. Proteins: Struct Funct Bioinformatics 2005;58:119–125.
15. Katoh E, Louis JM, Yamazaki T, Gronenborn AM, Torchia DA, Ishima R. A solution NMR study of the binding kinetics and the internal dynamics of an HIV-1 protease-substrate complex. Protein Sci 2003;12:1376–1385.
16. Ala PJ, Huston EE, Klabe RM, Jadhav PK, Lam PYS, Chang CH. Counteracting HIV-1 protease drug resistance: structural analysis of mutant proteases complexed with XV638 and SD146, cyclic urea amides with broad specificities. Biochemistry 1998;37:15042–15049.
17. Ala PJ, Huston EE, Klabe RM, McCabe DD, Duke JL, Rizzo CJ, Korant BD, DeLoskey RJ, Lam PYS, Hodge CN, Chang CH. Molecular basis of HIV-1 protease drug resistance: structural analysis of mutant proteases complexed with cyclic urea inhibitors. Biochemistry 1997;36:1573–1580.
18. Shafer RW, Stevenson D, Chan B. Human immunodeficiency virus reverse transcriptase and protease sequence database. Nucleic Acids Res 1999;27:348–352.
19. Shafer RW, Vuitton DA. Highly active antiretroviral therapy (HAART) for the treatment of infection with human immunodeficiency virus type 1. Biomed Pharmacother 1999;53:73–86.
20. Erickson JW, Burt SK. Structural mechanisms of HIV drug resistance. Ann Rev Pharmacol Toxicol 1996;36:545–571.
21. Wang W, Kollman PA. Computatioinal study of protein specificity: The molecular basis of HIV-1 protease drug resistance. Proc Natl Acad Sci USA 2001;98:14937–14942.
22. Hong L, Zhang XJC, Hartsuck JA, Tang J. Crystal structure of an in vivo HIV-1 protease mutant in complex with saquinavir: insights into the mechanisms of drug resistance. Protein Sci 2000;9:1898–1904.
23. Piana S, Carloni P, Rothlisberger U. Drug resistance in HIV-1 protease: flexibility-assisted mechanism of compensatory mutations. Protein Sci 2002;11:2393–2402.
24. Clemente JC, Moose RE, Hemrajani R, Whitford LRS, Govindasamy L, Reutzel R, McKenna R, Agbandje-McKenna M, Goodenow MM, Dunn BM. Comparing the accumulation of active- and non-active-site mutations in the HIV-1 protease. Biochemistry 2004;43:12141–12151.
25. Maschera B, Darby G, Palu G, Wright LL, Tisdale M, Myers R, Blair ED, Furfine ES. Human immunodeficiency virus—mutations in the viral protease that confer resistance to saquinavir increase the dissociation rate constant of the protease-saquinavir complex. J Biol Chem 1996;271:33231–33235.
26. Perryman AL, Lin JH, McCammon JA. HIV-1 protease molecular dynamics of a wild-type and of the V82F/I84V mutant: possible contributions to drug resistance and a potential new target site for drugs. Protein Sci 2004;13:1108–1123.
27. Hornak V, Okur A, Rizzo RC, Simmerling C. HIV-1 protease flaps spontaneously open and reclose in molecular dynamics simulations. Proc Natl Acad Sci USA 2006;103:915–920.
28. Rose RB, Craik CS, Stroud RM. Domain flexibility in retroviral proteases: structural implications for drug resistant mutations. Biochemistry 1998;37:2607–2621.
29. Logsdon BC, Vickrey JF, Martin P, Proteasa G, Koepke JI, Terlecky SR, Wawrzak Z, Winters MA, Merigan TC, Kovari LC. Crystal structures of a multidrug-resistant human immunodeficiency virus type 1 protease reveal an expanded active-site cavity. J Virol 2004;78:3123–3132.
30. Liu HY, MullerPlathe F, vanGunsteren WF. A combined quantum/classical molecular dynamics study of the catalytic mechanism of HIV protease. J Mol Biol 1996;261:454–469.
31. Piana S, Carloni P. Conformational flexibility of the catalytic Asp dyad in HIV-1 protease: an ab initio study on the free enzyme. Proteins: Struct Funct Genet 2000;39:26–36.
32. Fornabaio M, Spyrakis F, Mozzarelli A, Cozzini P, Abraham DJ, Kellogg GE. Simple, intuitive calculations of free energy of binding for protein-ligand complexes. III. The free energy contribution of structural water molecules in HIV-1 protease complexes. J Med Chem 2004;47:4507–4516.
33. Chen XF, Weber IT, Harrison RW. Molecular dynamics simulations of 14 HIV protease mutants in complexes with indinavir. J Mol Model 2004;10:373–381.
34. Kovalevsky AY, Tie YF, Liu FL, Boross PI, Wang YF, Leshchenko S, Ghosh AK, Harrison RW, Weber IT. Effectiveness of nonpeptide clinical inhibitor TMC-114 on HIV-1 protease with highly drug resistant mutations D30N, I50V, and L90M. J Med Chem 2006;49:1379–1387.
35. Marrone TJ, Resat H, Hodge CN, Chang CH, McCammon JA. Solvation studies of DMP323 and A76928 bound to HIV protease: analysis of water sites using grand canonical Monte Carlo simulations. Protein Sci 1998;7:573–579.
36. Spinelli S, Liu QZ, Alzari PM, Hirel PH, Poljak RJ. The 3-Dimensional structure of the Aspartyl protease from the HIV-1 isolate bru. Biochimie 1991;73:1391–1396.
37. MOE (Molecular Operating Environment), version 2006.06. Montreal, Canada: Chemical Computing Company; 2006.

 DOI 10.1002/prot

38. Case DA, Pearlman DA, Caldwell JW, Wang J, Ross WS, Simmerling CL, Darden TA, Mertz KM, Stanton RV, Cheng AL, Vincent JJ, Crowley M, Tsue V, Gohlke H, Radmer R, Duan Y, Pitera J, Massova I, Seibel GL, Singh C, Weiner P, Kollman PA. AMBER Simulation Software Package, version 7, Vol. 2006. San Francisco, CA: University of California; 2002.
39. Schafmeister CEAF, Ross WS, Romanovski V. LEap Software Package. San Fransciso, CA: University of California; 1995.
40. Berendsen HHC, Postma JPM, Gunsteren WF, DiNola A, Haak JR. Molecular dynamics with coupling to an external bath. J Chem Phys 1984;81:3684–3690.
41. Essmann U, Perera L, Berkowitz ML, Darden T, Lee H, Pedersen LG. A smooth particle mesh ewald method. J Chem Phys 1995;103: 8577–8593.
42. Cox TF, Cox MAA. Multidimensional scaling. Boca Raton: Chapman & Hall; 2001.
43. Amadei A, Linssen ABM, Berendsen HJC. Essential dynamics of proteins. Proteins: Struct Funct Genet 1993;17:412–425.
44. Garcia AE. Large-amplitude nonlinear motions in proteins. Phys Rev Lett 1992;68:2696–2699.
45. Lou H. Analyzer, 1.0. East Lansing; 2005.
46. Piana S, Carloni P, Parrinello M. Role of conformational fluctuations in the enzymatic reaction of HIV-1 protease. J Mol Biol 2002;319:567–583.
47. Miller M, Schneider J, Sathyanarayana BK, Toth MV, Marshall GR, Clawson L, Selk L, Kent SBH, Wlodawer A. Structure of complex of synthetic HIV-1 protease with a substrate-based inhibitor at 2.3-a resolution. Science 1989;246:1149–1152.
48. Northrop DB. Follow the protons: a low-barrier hydrogen bond unifies the mechanisms of the aspartic proteases. Acc Chem Res 2001;34:790–797.
49. Rick SW, Erickson JW, Burt SK. Reaction path and free energy calculations of the transition between alternate conformations of HIV-1 protease. Proteins: Struct Funct Bioinformatics 1998;32:7–16.
50. Freedberg DI, Ishima R, Jacob J, Wang YX, Kustanovich I, Louis JM, Torchia DA. Rapid structural fluctuations of the free HIV protease flaps in solution: relationship to crystal structures and comparison with predictions of dynamics calculations. Protein Sci 2002;11:221–232.
51. Condra JH, Schleif WA, Blahy OM, Gabryelski LJ, Graham DJ, Quintero JC, Rhodes A, Robbins HL, Roth E, Shivaprakash M, Titus D, Yang T, Teppler H, Squires KE, Deutsch PJ, Emini EA. In-vivo emergence of HIV-1 variants resistant to multiple protease inhibitors. Nature 1995;374:569–571.
52. Collins JR, Burt SK, Erickson JW. Flap opening in HIV-1 protease simulated by activated molecular-dynamics. Nat Struct Biol 1995;2: 334–338.
53. Chen ZG, Li Y, Schock HB, Hall D, Chen E, Kuo LC. 3-Dimensional structure of a mutant HIV-1 protease displaying cross-resistance to all protease inhibitors in clinical-trials. J Biol Chem 1995; 270:21433–21436.
54. Mahalingam B, Louis JM, Hung J, Harrison RW, Weber IT. Structural implications of drug-resistant mutants of HIV-1 protease: high-resolution crystal structures of the mutant protease/substrate analogue complexes. Proteins: Struct Funct Genet 2001;43:455–464.
55. Hong L, Zhang X, Foundling S, Hartsuck JA, Tang J. Structure of a G48H mutant of HIV-1 protease explains how glycine-48 replacements produce mutants resistant to inhibitor drugs. FEBS Lett 1997;420:11–16.
56. Wittayanarakul K, Aruksakunwong O, Saen-oon S, Chantratita W, Parasuk V, Sompornpisut P, Hannongbua S. Insights into saquinavir resistance in the G48V HIV-1 protease: quantum calculations and molecular dynamic simulations. Biophys J 2005;88:867–879.
57. Hong L, Treharne A, Hartsuck JA, Foundling S, Tang J. Crystal structures of complexes of a peptidic inhibitor with wild-type and two mutant HIV-1 proteases. Biochemistry 1996;35:10627–10633.
58. Bjelic S, Aqvist J. Catalysis and linear free energy relationships in aspartic proteases. Biochemistry 2006;45:7709–7723.
59. Smith R, Brereton IM, Chai RY, Kent SBH. Ionization states of the catalytic residues in HIV-1 protease. Nat Struct Biol 1996;3:946–950.
60. Suguna K, Padlan EA, Smith CW, Carlson WD, Davies DR. Binding of a reduced peptide inhibitor to the aspartic proteinase from Rhizopus-Chinensis—implications for a mechanism of Action. Proc Natl Acad Sci USA 1987;84:7009–7013.